

Appendix A

Toward the computational design of a novel enantioselective hydrolase

Abstract

Enzymes are ideal catalysts of organic reactions because of their high efficiency and ability to perform a wide variety of chemical transformations with extreme chemo- and enantioselectivity under mild reaction conditions. The chemical repertoire of natural enzymes is not exhaustive, however, and certain reactions of industrial interest are not found in nature. A general method to design and optimize an enzyme for the catalysis of a specific reaction, especially difficult enantioselective reactions, would be a powerful tool in organic synthesis and would open up a range of reactions not currently accessible due to the lack of an appropriate catalyst. Towards this end, we used the ORBIT computational protein design software in an attempt to design an enzymatic catalyst for the kinetic resolution of N-benzoyl-L-phenylalanine through the selective hydrolysis of (S)-2-benzyl-4-phenyl-oxazolone-5-one (F-FOX) as a model system. This project did not result in an active enzyme. However, the methods developed here laid the groundwork for future active designs using other systems.

Introduction

Enantioselective enzymes

Enantiomerically pure drugs have become the new standard in the pharmaceutical industry. Chemists have long recognized the influence chiral molecules can have over a biological system. Indeed, many of the common drugs isolated from natural sources, such as morphine and quinine, are single enantiomers.¹ However, synthetically producing the single active enantiomer of a compound has always been challenging, if not impossible, and as a result, chiral drugs were historically produced as racemates.^{2,3} Since the tragic effects of thalidomide were discovered in 1961, we have come to better understand the differing biological activity and pharmacokinetics of the individual enantiomers of a drug. These differences make enantiopure drugs preferable and even necessary in many cases. Fortunately, technology has advanced to make the synthesis of many single enantiomer drugs possible.³

Chemists use four basic methods to enantiomerically enrich a target compound: (1) isolation of chiral compounds from nature, (2) chemical asymmetric techniques, (3) chiral resolutions, and (4) enzymatic techniques. In spite of major advances in asymmetric synthetic techniques, nature is still arguably the richest source of chiral compounds and catalysts. However, even with this “chiral pool” of compounds, the selection, enantiopurity, and extractable quantities of these chiral compounds are limited.⁴ Asymmetric strategies to access chiral compounds are far from being fully developed. Especially challenging reactions involve the formation of carbon-carbon bonds to a stereogenic center. Chiral resolutions of racemates into individual enantiomers are one of the oldest and most industrially important methods for enantio-enrichment. However,

this approach has the inherent drawback of a maximum theoretical yield of 50%, because by definition a racemate only has 50% of the desired enantiomer, except in special cases described below.^{5,6}

With an ever-increasing demand for enantiomerically pure, complex, biologically active compounds (i.e., drugs), synthetic chemists are necessarily beginning to look beyond standard chemical strategies in favor of the high yields, efficiency, and strict selectivity of enzymatic reactions.² Although enzymes are widely used in industry, their use is often limited to reactions that are parts of natural metabolic processes. Exceptions include enzymes with natural limited selectivity such as some lipases.⁷

As previously mentioned in Chapter I, both directed evolution and catalytic antibodies have drawbacks that prevent their use as general tools for the introduction of new chemistries into enzymes. Here, I describe our initial strategy to introduce enantioselective hydrolysis activity into inert scaffolds using our computational protein design software, ORBIT.

Selected system: the dynamic kinetic resolution of F-FOX hydrolysis

Dynamic kinetic resolutions are a powerful method for transforming a racemic starting material into an enantiomerically pure product without the theoretical yield limitations imposed by standard chiral resolutions. Under the conditions of a dynamic kinetic resolution, the starting material racemizes and an equilibrium is established between the stereoisomers.⁶ Consequently, by continuously removing one enantiomer from the mixture, 100% of the starting material can be converted into the desired enantiomer of the product compound. Our goal here was to design a stereoselective

enzyme to carry out a dynamic kinetic resolution. The enantioselective hydrolysis of (S)-2-benzyl-4-phenyl-oxazolin-5-one (F-FOX) to produce *N*-benzoyl-L-phenylalanine⁸ was chosen as our model system (Figure A-1).

Initially, we found F-FOX hydrolysis to be an attractive system for this proof of principle because (1) F-FOX has reasonable solubility and stability in water;⁹ (2) oxazolones have a characteristic absorption at around 245 nm that is reduced significantly upon hydrolysis, allowing the reaction to be easily monitored (see Materials and Methods); (3) F-FOX can be easily synthesized through a single-step reaction from commercially available materials;¹⁰ (4) F-FOX racemizes quickly under basic conditions in aqueous solution (Figure A-3C);¹¹ (5) the benzyl sidechain of F-FOX gives a large hydrophobic handle with which to distinguish two enantiomers; (6) F-FOX is fairly rigid for its size, having only three degrees of freedom to model in the transition state; (7) F-FOX undergoes hydrolysis by a simple base-catalyzed mechanism;^{9,11} (8) F-FOX is a strong fluorophore in aqueous solution providing a possible method for binding analysis fluorimetry (see Results); (9) F-FOX hydrolysis is not performed selectively by a natural enzyme. Some lipases have been shown to hydrolyze oxazolones, but these enzymes are nonselective hydrolases, the hydrolysis rates are modest, and the mechanism of oxazolone hydrolysis has not been established.^{12,13}

In a method analogous to the generation of catalytic antibodies, our strategy was to first calculate a structure for the F-FOX transition state and then optimize the binding pocket of a protein around the structure using ORBIT to maximize the protein's affinity for the transition state.

Scaffold selection

In contrast to directed evolution, the protein design process requires a scaffold that is inert with respect to the reaction of interest. Several proteins were tested computationally as possible scaffolds to house the F-FOX hydrolase active site and transition state including *Homo sapien* retinol binding protein (PDB: 1BRP),¹⁴ *E. coli* ribose binding protein (PDB: 2DRI),¹⁵ *Thermus thermophilus* aspartate amino transferase (PDB: 1GCK),¹⁶ and *E. coli* maltose binding protein (pdb: 1ANF).¹⁷ As these proteins are all enzymes or ligand-binding proteins, they all have well-defined ligand-binding pockets, which is where the active site search was targeted. The periplasmic binding protein maltose binding protein (MBP) from *E. coli*, shown in Figure A-2, was chosen as the initial scaffold for the F-FOX hydrolase design because the size and shape of its binding pocket can accommodate the necessary catalytic residues and reaction transition state. Another attractive feature of this protein is its large size (41 kDa). In general, large proteins are convenient for enzyme design because the overall stability of the protein should not be significantly affected by mutations introduced to the binding pocket. Also, MBP not only binds to maltose with high affinity, but also binds to maltotriose and maltotetraose. The F-FOX transition state is of similar size and shape to maltose and maltotriose, suggesting that with some modifications to the residues within the binding pocket, MBP should be capable of binding to the F-FOX transition state as well. Our design calculations were based on the MBP crystal structure in complex with maltose at 1.67 Å resolution (PDB: 1ANF).¹⁷

Materials and Methods

Calculation of F-FOX transition state

Ab initio calculations of the first transition state of (S)-F-FOX hydrolysis (Figure A-1) were performed using the hybrid density functional B3LYP as implemented by the Jaguar 5.5 program package¹⁸ and a 6-31G** basis set. The implicit solvation effects of methanol were calculated using a dielectric constant of 33.62 and a probe radius of 2.00 Å. Partial atomic charges were calculated with an electrostatic potential fit.

The system under investigation included the (S)-F-FOX structure with the phenyls removed to facilitate a faster calculation, a water molecule, and NH₃ to deprotonate the attacking water (Figure A-3A). A transition state structure for the hydrolysis of (S)-F-FOX was calculated using the following steps. First, a bond length scan was performed by varying the distance between the attacking water molecule and the carbonyl carbon of F-FOX until a maximum energy was found. The distance that produced the highest energy structure was used as the starting point for the transition state calculation. The final transition state structure has a water-oxygen to carbonyl-carbon distance of 1.79 Å (Figure A-3B). We made 18 conformations of the transition state structure by varying the χ_1 and χ_2 angles of the benzyl group to correspond to the six phenylalanine rotamers in the Karplus and Dunbrack library¹⁹ and by allowing the phenyl ring attached directly to the oxazolone to adopt positions that are $\pm 15^\circ$ out of the oxazolone plane as shown in Figure A-3C. The partial atomic charges for F-FOX were also calculated with Jaguar using an electrostatic potential fit.

Defining the design geometric constraints

To obtain a protein that exhibits high affinity and specificity towards the transition state structure, optimal contacts and ranges of contacts were defined between the transition state structure and three amino acid side chains based on ideal hydrogen bond configurations (Figure A-4). The geometric constraints shown in Figures 3-5 and 3-6 describe the activation of water by both the N δ and N ϵ atoms of neutral histidine (in the Hie form of histidine, N ϵ is protonated; in Hid, N δ is protonated) and the protonation of the oxazolone nitrogen by either nitrogen of protonated histidine (Hsp). Each of the constraints of these geometry definitions defines a range of allowable distances, angles or torsions among the atoms of the transition state and the side chain.

If the molecules adopt any orientation whose geometry falls within these ranges, they will be considered to be making a hydrogen bonding contact. There are four different ways the arginine guanidinium group can make a double hydrogen bonding contact to the two oxygens of the transition state (Figure A-6A) and the geometric constraints for arginine-transition state contacts are shown in Figure A-6B. To help define the geometries, pseudo-atoms with no volume, mass, or charge were created at the midpoint between each pair of nitrogens and between the two oxygens of the transition state (shown as pink stars in the figures). The distance between the pseudo-atom at the optimal orientation for the formation of two hydrogen bonds is 2.9 Å.

Design strategy and parameters

The overall strategy for the enzyme design was: (1) strip the side chains from the binding pocket, (2) find locations within the binding pocket that will allow all of the

defined contacts between the catalytic side chains and the transition state, (3) choose the optimal location for the active site, and (4) repack the rest of the binding pocket side chains around the catalytic residues and transition state. Steps 1-3 are referred to as the active site search and step 4 is called active site repacking.

As described previously, the scoring function is the sum of the van der Waals energy, hydrogen bond energy, electrostatics energy, and atomic solvation energy for the system. The atomic radii used to calculate the van der Waal's energies were scaled by 0.95.²⁰ Making the atoms appear smaller than their known van der Waal's radius softens all of the interactions and serves to compensate for the rigidity of the fixed backbone and discrete rotamers. We used a hydrogen bond potential function with a well depth of 8 kcal/mol.²¹ Hydrogen bonds between two side chains and between a side chain and a remote backbone atom were treated equally, but hydrogen bonds between a side chain and its own backbone are not considered stabilizing and were scaled by 0.00. The surface area-based solvation terms were all weighted individually:²² the benefit for non-polar surface area burial was 0.026 kcal/mol/Å², the penalty for nonpolar surface area exposure was scaled by a factor of 1.60, and the penalty for burial of polar atoms was 0.10 kcal/mol/Å².

The side chains were removed from all of the residues of MBP within 4 Å of maltose in the wild-type structure, creating a poly-glycine hole in the binding pocket. The residues within 8 Å of maltose in the wild-type structure were allowed to change conformation but not identity during the active site search. All other side chains and the backbone atoms were kept in the positions determined by the crystal structure. The geometry definitions for the Hie/Hid to transition state contact are special in that they

were also used to define rotamers for the transition state with respect to each neutral histidine rotamer. As these “substrate-target” residues sample positions/rotamers during the transition state search, the transition state structure samples all of its rotameric forms as it translates and rotates with respect to the neutral histidine rotamer. These translations and rotations were subject to the geometric constraints shown in Figure 4. Distances were sampled in 0.5 Å steps, and angles and torsions were sampled in 15 or 20° steps. The two additional catalytic residues also sampled positions within the poly-glycine region.

Active site search

In the active site search, single residue and pair-wise energies were calculated without application of solvation potentials. Any configuration meeting all the geometric constraints discussed above received an energy benefit of 100 kcal/mol, biasing the resulting configurations towards those that have a desired geometry with respect to the transition state. A penalty of 1000 kcal/mol was applied to any arginine or histidine located within the binding pocket that does not make a specified contact to the transition state, preventing extra catalytic residues from being selected based on favorable van der Waals interactions with the backbone or other residues. Optimization was performed using a modification of the FASTER algorithm,²³ resulting in a solution that specifies a single possible location of the active site.

A Monte Carlo search^{24,25} was then performed to explore the “active site space” around the FASTER solution. To surmount the unrealistically deep local minima represented by a three-residue active site/transition state configuration within an empty

pocket, an increased high annealing temperature of 500,000 K was used. Even with this elevated temperature, only about 50% of the moves were successful. The Monte Carlo search provided a list of sequences that met all of the specified geometric and sequence requirements, ranked by energy; these structures were then evaluated individually. Evaluation criteria included transition state/catalytic residue geometry, favorable interactions of the catalytic residues with the backbone, wild-type residue identity at a catalytic residue position, positioning of the catalytic residues within the binding pocket and relative to one another, and overlap of the transition state structure with the position of the natural ligand within the binding pocket.

After the optimal active site location was chosen, the catalytic residue positions were fixed and FASTER was used to repack the rest of the binding pocket side chains around the catalytic residues and the transition state structure. Binding pocket residues capable of contacting the transition state or the catalytic residues could sample rotamers for all the amino acids except proline, methionine, and cysteine. The transition state was allowed to move in small steps according to its allowed geometries with respect to the neutral histidine. All other binding pocket residues and the catalytic residues were allowed to sample all conformations but were not allowed to change identity. Again, a Monte Carlo algorithm was used to sample sequence space around the solution provided by FASTER. A high annealing temperature of 4000 K was used. The top 20 Monte Carlo sequences were then subjected to a DEE-based algorithm that finds the lowest energy rotamer for each designed residue in the sequence.

F-FOX synthesis and characterization

F-FOX was synthesized as previously described¹⁰ and purified via flash chromatography. (230-400 mesh silica gel, 60 Å purchased from Aldrich, 4:7 ethyl acetate:hexanes). *N*-benzoyl-L-phenylalanine and *N*-cycloheptyl-*N'*-2-(*N*-methyl morpholino)-ethylcarbodiimide *p*-toluenesulfonate were purchased from Aldrich and used without further purification. Evaporation under reduced pressure gave the oxazolone as a white solid; yield: 80.0 mg (50%) m.p. 70-72°C (Lit.¹⁰ m.p. 70-71°C).

I.R. (CH₂Cl₂): ν = 1822; 1655; 1496; 1425; 1323; 1082; 1046; 965; 885 cm⁻¹.

¹H-N.M.R. (CDCl₃): δ = 3.3 (q, 2H); 4.7 (t, 1H); 7.4 (t, 2H); 7.6 (d, 1H); 7.9 ppm (d, 2H).

NMR was performed on a Varian Mercury 300 MHz machine, and IR spectra were recorded using a Perkin-Elmer Spectrum BX spectrometer. UV-vis spectroscopy was performed using a Shimadzu UV-1601 spectrophotometer equipped with a temperature controlled cell holder. Fluorescence measurements were performed on a Photon Technology International fluorimeter equipped with a Model 180/814 photomultiplier detection system and a Ushio xenon short arc lamp. Fluorescence polarization experiments were carried out with 50 μ M to 0.5 nM protein and 500 nM F-FOX. 500 nM BSA was used as a control.

Protein expression and purification

The gene for the F-FOX hydrolase (1ANF-FFH) was optimized for expression, synthesized with an N-terminal His₆ tag and Gly-Gly-Ser linker (Blue Heron, Bothell, WA), and cloned into a pET11a vector (Invitrogen). The plasmid was transformed into

BL-21(DE3) Gold cells (Stratagene) by heat shock and protein expression was induced for 4 hours at 37°C with 1.0 mM IPTG. Cells were harvested by centrifugation at 5000 × g for 30 min and pellets were resuspended in 10 mM imidazole, 300 mM NaCl, 20 mM Tris pH 7.4. The cells were lysed mechanically and pelleted at 10,000 × g for 45 min. The soluble fraction was applied to a Ni-NTA Agarose column (QIAGEN) and washed with 10 column volumes of 10 mM imidazole, 300 mM NaCl, 20 mM Tris pH 7.4 and 10 column volumes of 20 mM imidazole, 300 mM NaCl, 20 mM Tris pH 7.4. The protein was eluted with 250 mM imidazole, 300 mM NaCl, 20 mM Tris pH 7.4 and the eluate was dialyzed exhaustively against 20 mM Tris pH 7.4, 50 mM NaCl and stored at 4°C until use. The overall purity of 1ANF-FFH was > 90% as determined by SDS-PAGE. The expected molecular weight of 1ANF-FFH was within 9 units of the weight determined by electrospray mass spectrometry. Expression yields for 1ANF-FFH were between 20 and 40 mg per liter of culture.

Circular dichroism

Circular dichroism (CD) data were recorded with an Aviv DS spectropolarimeter. The temperature was controlled with a thermoelectric unit. Experiments were performed on samples containing 16.6 μM protein in buffer containing 20 mM Tris pH 7.4 and 50 mM NaCl. Wavelength scans were performed in triplicate in 1nm steps from 250 nm to 190 nm with an averaging time of 1 sec. Thermal denaturation was performed in 1°C steps from 1 to 99°C with 2 min of equilibration at each new temperature and averaging over 30 sec. Thermal unfolding was monitored at 222 nm. Apparent melting temperatures were determined using the relation of Minor and Kim.²⁶

Enzyme activity assays

Enzymatic activity was assayed using 3-5 μM 1ANF-FFH in 1 mL total volume and buffers of varying composition, salt concentration, pH and temperature. The assay was initiated by the addition of F-FOX in acetonitrile to a final concentration of 20–70 μM . If the assay temperature was above 25°C, the protein and the buffer (or the buffer and an equivalent amount of the protein storage buffer for controls) were equilibrated at that temperature for 10 min before the addition of substrate. The disappearance of the substrate with respect to time was observed by monitoring the absorbance of the sample at 245 nm for 10 min at each initial substrate concentration. Initial substrate concentrations were calculated using an extinction coefficient of 13000 $\text{cm}^{-1}\text{M}^{-1}$ (see Results section). The initial rates were calculated from the linear portion of the substrate concentration versus time curves. For preliminary enzyme activity assays, all rate constants were determined at three different initial substrate concentrations.

Fluorescence polarization

Fluorescence polarization measurements were performed on a Photon Technology International fluorimeter equipped with a Model 180/814 photomultiplier detection system, a Ushio xenon short arc lamp, and three polarizers from Photon Technology International. An excitation wavelength of 356 nm and an emission wavelength of 440 nm were used. Data were collected for 60 sec with a slit width of 1.25 mm. Experiments were carried out with 50 μM to 0.5 nM protein and 500 nM F-FOX. BSA was used as a positive control.

Chiral HPLC

A method for the separation of D-benzoyl-phenylalanine and L-benzoyl-phenylalanine (the products of F-FOX hydrolysis) was developed using chiral high-pressure liquid chromatography (HPLC). Good separation was found in 12% ethanol in hexanes with 0.1% trifluoroacetic acid on a 4.6 mm × 250 mm Chiracel AD column at a flow rate of 1 mL/min.

Site-directed mutagenesis

All mutagenesis reactions were carried out using site-directed mutagenesis as described in Chapter III, Materials and Methods.

Results and Discussion

F-FOX characterization

The UV-vis spectra of F-FOX and N-benzoyl-phenylalanine are shown in Figure A-7. The spectra are substantially different, but both the F-FOX reactant and benzoyl-phenylalanine product absorb at the same wavelengths. Because a large difference in the two spectra occurs at 245 nm, this wavelength was chosen to follow the reaction kinetics. F-FOX and N-benzoyl-phenylalanine were determined experimentally to have extinction coefficients of $13000 \pm 311 \text{ cm}^{-1}\text{M}^{-1}$ and $6600 \pm 141 \text{ cm}^{-1}\text{M}^{-1}$, respectively, at 245 nm (data not shown).

The hydrolysis of F-FOX follows pseudo-first-order kinetics with a large dependence on pH. The background reaction occurs with a first-order rate constant of

$0.00836 \pm 0.000495 \text{ min}^{-1}$ in 0.01 M KPi pH 6.6. As expected, the rate constant is positively correlated with pH (data not shown).

An excitation wavelength scan shows that F-FOX fluoresces upon excitation with 356 nm light with emission occurring at 440 nm. This fluorescence is strongly pH dependent (Figure A-8), suggesting that F-FOX fluoresces most strongly when it is in its deprotonated form. The loss of the acidic α -proton causes aromaticity to extend between the oxazolone and the phenyl side chain, facilitating fluorescence.

Due to the very different character of the two forms of F-FOX, its fluorescence is also strongly dependent on the nature of its environment. The fluorescence of F-FOX is completely quenched upon transfer into dichloromethane or acetonitrile, but it regains fluorescence with increasing water concentration in a mixture with acetonitrile. In contrast, most fluorescent molecules experience an increase in fluorescence in hydrophobic environments because these types of environments tend to shield the molecule from quenchers that are present in aqueous solutions.²⁷ Because the hydrophobic binding pockets of proteins can mimic the effects seen in nonpolar solvents, we attempted to take advantage of this unusual fluorescence property of F-FOX to monitor F-FOX-protein binding through a decrease in fluorescence. However, an assay of this type is challenging because many factors other than a change in the environment of a fluorophore can contribute to a reduction in fluorescence. In addition, measurements of a reduction in fluorescence are inherently less sensitive than measurements of an increase in fluorescence.

1ANF-FFH active site

Of the many possible active site locations, one was ultimately chosen by visual inspection. This site is shown in Figure A-9A. In this active site, all three catalytic residues make good hydrogen bonds to the transition state. N ϵ of Arg 66 forms an electrostatically favorable contact with the carbonyl oxygen of the transition state, which at 4.1 Å, is too long to call a true hydrogen bond. This particular contact may be important in stabilizing the oxyanion intermediate of the hydrolysis, and the long contact may give the transition state enough room to form the intermediate. In addition to the favorable geometry between the catalytic residues and the transition state, this particular active site was chosen because of the similarity of the rotameric forms of the designed residues and the wild-type residue (Figure A-9C). Hid 62 overlays perfectly with the indole of the wild-type Trp, and Arg 66 is not only a wild-type residue, but adopts a very similar rotamer to that in the crystal structure.

The similarity of the catalytic residues and wild-type residues is promising, suggesting that rotameric strain will not be a large destabilizing factor in the formation of this active site. Some of the catalytic residues of this active site also have additional stabilizing interactions. Hid 64 makes an additional hydrogen bond contact to a main chain carbonyl that was not required by the geometry definitions (Figure A-9B). This extra contact may stabilize the catalytic histidine in its appropriate orientation. The final design for the F-FOX hydrolase based on scaffold 1ANF (1ANF-FFH) is a seven-fold mutant including the two catalytic histidines. The catalytic arginine at position 66 is wild type. Figure A-10A shows the designed active site overlaid with the wild-type residues. Again, all of the designed residues adopt rotamers similar to those in the wild-type

protein. A space-filling representation of the active site and the binding pocket residues (Figure A-10B) shows that the benzyl side chain of the transition state is well packed. Favorable van der Waals contacts are made with designed residues such as Hid 64 and Phe 63 as well as with wild-type residues such as Tyr 155, Trp 230, and Trp 340.

CD analysis of 1ANF-FFH

CD analysis of 1ANF-FFH shows that the protein is well folded and has an overall secondary structure composition comparable to that of wild-type MBP (Figure A-11A). Difference in the curve magnitudes may be due to uncertainties in protein concentrations. The apparent melting temperature of 1ANF-FFH is very close to the melting temperature determined for MBP under identical conditions ($58.3 \pm 0.03^\circ\text{C}$ for 1ANF-FFH versus $60.2 \pm 0.05^\circ\text{C}$ for MBP as determined by thermal denaturation) (Figure A-11B). The similarity in melting temperatures indicates that the seven mutations introduced into the binding pocket of MBP have little effect on the overall stability of the protein.

Enzyme assays

The apparent pseudo-first-order rate constants determined for F-FOX hydrolysis under various conditions are shown in Table A-1 and Figure A-12. The addition of micromolar quantities of 1ANF-FFH was found to increase the rate of F-FOX hydrolysis up to 10% above background at 25°C , which is similar to the rate enhancement seen upon addition of wild-type MBP. A rate increase of this size is not indicative of enzymatic activity and a similar effect upon addition of wild-type protein suggests that F-FOX

hydrolysis is being affected subtly by nonspecific interactions with the exterior of the protein. Pseudo-first-order rate constants were also established for the background hydrolysis of F-FOX in buffer and in buffer with 50 μ M imidazole. The addition of imidazole did not enhance F-FOX hydrolysis significantly at any pH. An increase in buffer concentration from 10 mM to 50 mM results in an increase in F-FOX hydrolysis consistent with general base catalysis, but the addition of 1ANF-FFH and MBP do not increase the rate significantly in either case. Assays performed at 37°C show an increase in the rate of background hydrolysis compared to 25°C, but no significant rate enhancement was observed by the addition of 1ANF-FFH (data not shown).

FOX binding assay

1ANF-FFH did not show any FOX hydrolysis activity. However, FOX may have still been binding in the active site of 1ANF-FFH. Taking advantage of FOX fluorescence, fluorescence anisotropy was used to assay FOX binding. MBP has a large, irregular shape, so the effective size of FOX should increase dramatically upon being bound by the protein, resulting in an increase in its fluorescence anisotropy. As mentioned in the Methods, FOX fluorescence decreases in nonpolar solvents. The binding pocket of the protein is less polar than water, so FOX fluorescence is expected to decrease upon entering the binding pocket. The decrease in FOX fluorescence upon protein binding, along with the high background hydrolysis rate of FOX, make this measurement more difficult because both result in a decrease in signal. BSA was used as a control because it is known to have the ability to bind nonspecifically to many small molecules, especially hydrophobic small molecules.²⁸

The titration of 1ANF-FFH at a constant FOX concentration is shown in Figure A-13. The titration curve shows that 1ANF-FFH binds to FOX much more weakly than BSA, which probably exhibits nonspecific binding. It is unclear if this weak 1ANF-FFH binding is specific or nonspecific.

1ANF-FFH modifications

In our analysis of the model of the inactive design, we identified four potentially beneficial mutations for 1ANF-FFH (Figure A-13). These include a double mutation of I239 and A96 to tryptophan at positions located in the hinge region distal to the ligand-binding site. Hellinga and coworkers reported that this double mutant induces a 60-fold increase in the affinity of wild-type MBP for maltose by shifting the equilibrium of MBP to its closed conformation.²⁹ We predicted that the N150D mutation would contribute to the stabilization of the protonated catalytic histidine in the desired configuration and protonation state. Two additional mutations, (Y155F) and another double mutant of polar residues to tryptophan (N12W and D14W) were not expected to directly influence the catalytic residues or transition state, but might contribute to the stabilization of the binding pocket itself (Figure A-13). These mutations were made using site-directed mutagenesis (see Materials and Methods) and the activity of the variants was assayed as described above. The N150D mutant and the A96W/I329W double mutant showed no significant F-FOX hydrolysis activity (Figure A-14). The N12W/D14W double mutant and the N150D/A96W/I239W triple mutant also showed no significant activity (Figure A-15).

Lessons learned from F-FOX hydrolase design

None of the F-FOX hydrolase designs have significantly catalyzed F-FOX hydrolysis under any of the conditions examined so far. In retrospect, some issues have been identified that will help inform our future selection of both the chemical system and the scaffold. First, the protonation state of the catalytic histidines (especially the base) is critical to the proposed hydrolysis mechanism. However, histidine has a pKa near neutral and can exist in three protonation states, making it difficult to control the histidine species present in the active site. Second, the F-FOX hydrolysis system has a background reaction rate that is relatively high. This is a benefit in the sense that the reaction is easy to carry out. However, any designed enzyme would have to perform better than this high background rate before activity could be detected. Finally, the flexibility of some of the scaffolds selected for these designs (especially MBP) may lead to active sites that are too exposed to solvent. As mentioned above, the catalytic histidines must be in their correct protonation states for the reaction to work and the presence of water in the active site may cause the protonation state of the histidines to shift unpredictably. In addition, the active site of the MBP designs is not fully formed until the hinge that connects the two lobes is closed. For future designs, it would be advantageous to choose scaffolds that always have a fully formed active site rather than one that spends at least part of its time in an open state where entropy and desolvation costs work against the formation of the active site.

Because we have no structural data for any of these designs, we can only speculate on reasons for their inactivity. However, the problems listed above combine to

form a reasonable argument for abandoning this system in favor of one that has fewer practical issues.

Acknowledgements

We thank Jonas Oxgaard from the Goddard group for help in determining the transition state structure for the F-FOX reaction and for general guidance in the use of the Jaguar software. We also thank Daniel Caspi and Doug Behenna from the Stoltz lab at Caltech for their help in developing the chiral HPLC assay and Ariele Hanek in the Dougherty lab for advice about F-FOX synthesis and characterization. Robert Dirks from the Pierce lab helped with the fluorescence polarization assays. This work was supported by the Howard Hughes Medical Institute and the Defense Advanced Research Project Agency.

References

1. Rouhi, A. M., Chiral business. *Chem. Eng. News* **2003**, May, 45-55.
2. Schoemaker, H. E.; Mink., D.; Wubbolts, M. G., Dispelling the myths- Biocatalysts in industrial synthesis. *Science* **2003**, 299, 1694-1697.
3. Agranat, I.; Caner, H.; Caldwell, J., Putting chirality to work: The strategy of chiral switches. *Nat. Rev. Drug Discov.* **1992**, 1, 753-768.
4. Blaser, H.-U., The chiral pool as a source of enantioselective catalysts and auxiliaries. *Chem. Rev.* **1992**, 92, 935-952.
5. Trost, B. M., Asymmetric catalysis: An enabling science. *Proc. Natl. Acad. Sci. USA* **2004**, 101, 5348-5355.
6. El Gihani, M. T.; Williams, J. M. J., Dynamic kinetic resolutions. *Curr. Opin. Chem. Biol.* **1999**, 3, 11-15.
7. Jaeger, K.-E.; Eggert, T., Lipases for biotechnology. *Curr. Opin. Biotechnol.* **2002**, 13, 345-351.
8. Williams, A., The oxazolinone intermediate in the hydrolysis and aminolysis of N-benzyloxycarbonyl-glycine derivatives. *J. Chem. Soc., Perkin Trans. 1* **1975**, 2, 947-953.
9. Goodman, M.; Levine, L., Peptide synthesis via active esters. IV. Racemization and ring opening reactions of optically active oxazolones. *J. Am. Chem. Soc.* **1964**, 86, 2918-2922.
10. Hoyng, C.; McKena, M.; Walters, D., A convenient procedure for synthesis of derivatives of 2-oxazolin-5-one. *Synthesis-Stuttgart* **1982**, 3, 191-193.
11. Goodman, M.; Stuben, K. C., Amino acid active esters III. Base-catalyzed racemization of peptide active esters. *J. Org. Chem.* **1962**, 27, 3409-3416.
12. Brown, S. A.; Parker, M.-C.; Turner, N. J., Dynamic kinetic resolution: synthesis of optically active α -amino acid derivatives. *Tetrahedron: Asymmetry* **2000**, 11, 1687-1690.
13. Crich, J. Z.; Brieva, R.; Marquart, P.; Gu, R.-L.; Flemming, S.; Sih, C. J., Enzymatic asymmetric synthesis of α -amino acids. Enantioselective cleavage of 4-substituted oxazolin-5-ones and thiazolin-5-ones. *J. Org. Chem.* **1993**, 58, 3252-3258.
14. Zanotti, G.; Ottonello, S.; Berni, R.; Monaco, H. L., Crystal-structure of the trigonal form of human plasma retinol-binding protein at 2.5-Angstrom resolution. *Journal of Molecular Biology* **1993**, 230, 613-624.
15. Bjorkman, A. J.; Binnie, R. A.; Zhang, H.; Cole, L. B.; Hermodoss, M. A.; Mowbray, S. L., Probing protein-protein interactions- The ribose-binding protein in bacterial transport and chemotaxis. *Journal of Biological Chemistry* **1994**, 269, 30206-30211.
16. Ura, H.; Nakai, T.; Kawaguchi, S.; Miyahara, I.; Hirotsu, K.; Kuramitsu, S., Substrate recognition mechanism of thermophilic dual-substrate enzyme. *J Biochem-Tokyo* **2001**, 130, 89-98.
17. Quioco, F. A.; Spurlino, J. C.; Rodseth, L. E., Extensive features of tight oligosaccharide binding revealed in high-resolution structures of the maltodextrin transport/chemosensory receptor. *Structure* **1997**, 5, 997-1015.

18. Jaguar 5.5, Schrodinger, L.L.C., Portland, OR, **1991-2003**.
19. Dunbrak, R. L.; Karplus, M., Backbone-dependent rotamer library for proteins. *J. Mol. Biol.* **1993**, *230*, 543-574.
20. Dahiyat, B. I.; Mayo, S. L., Probing the role of packing specificity in protein design. *Proc. Natl. Acad. Sci. USA* **1997**, *94*, 10172-10177.
21. Dahiyat, B. I.; Gordon, B.; Mayo, S. L., Automated design of the surface positions of protein helices. *Protein Sci.* **1997**, *6*, 1333-1337.
22. Street, A. G.; Mayo, S. L., Pairwise calculation of protein solvent-accessible surface areas. *Folding & Design* **1998**, *3*, 253-258.
23. Desmet, J.; Spriet, J.; Lasters, I., Fast and accurate side-chain topology and energy refinement (FASTER) as a new method for protein structure optimization. *Proteins: Struct. Funct. Genet.* **2002**, *48*, 31-43.
24. Metropolis, N.; Rosenbluth, A. W.; Rosenbluth, M. N.; Teller, A. H., Equation of state calculations by fast computing machines. *J. Chem. Phys.* **1953**, *21*, 1087-1092.
25. Kirkpatrick, S.; Gelatt, C. D.; Vecchi, M. P., Optimization by simulated annealing. *Science* **1983**, *220*, 671-675.
26. Minor, D. L., Jr.; Kim, P. S., Measurement of the beta-sheet-forming propensities of amino-acids. *Nature* **1994**, *367*, 660-663.
27. Lakowicz, J. R., *Principles of Fluorescence Spectroscopy*, 2nd ed. Kluwer Academic/Plenum Publishers: New York, **1999**.
28. Kraghshansen, U., Molecular aspects of ligand binding to serum albumin. *Pharmacol. Rev.* **1981**, *33*, 17-53.
29. Marvin, J. S.; Hellinga, H. W., Manipulation of ligand binding affinity by exploitation of conformational coupling. *Nat. Struct. Biol.* **2001**, *8*, 795-798.

Table A-1. Apparent pseudo-first-order rate constants for F-FOX hydrolysis.
Standard errors were calculated from assays at multiple initial substrate concentrations.

pH	k, min^{-1}			
	50 mM KPi 50mM NaCl	+ 50 μM imidazole	+ 5 μM 1ANF-FFH	+ 5 μM MBP
6.2	0.013 \pm 0.0001	0.014 \pm 0.001	0.014 \pm 0.0006	0.017 \pm 0.004
6.4	0.016 \pm 0.0003	0.018 \pm 0.001	0.018 \pm 0.0003	0.021 \pm 0.002
6.6	0.020 \pm 0.0003	0.022 \pm 0.0008	0.022 \pm 0.0004	0.025 \pm 0.003
6.8	0.024 \pm 0.001	0.026 \pm 0.002	0.029 \pm 0.0006	0.030 \pm 0.0003
7.0	0.031 \pm 0.002	0.031 \pm 0.003	0.034 \pm 0.0011	0.035 \pm 0.0005
7.2	0.035 \pm 0.002	0.037 \pm 0.001	0.040 \pm 0.0004	0.042 \pm 0.0018
7.4	0.041 \pm 0.002	0.044 \pm 0.001	0.047 \pm 0.0018	0.050 \pm 0.002
7.6	0.047 \pm 0.002	0.05 \pm 0.002	0.052 \pm 0.0016	0.054 \pm 0.002

pH	k, min^{-1}			
	10 mM KPi 50mM NaCl	+ 50 μM imidazole	+ 5 μM 1ANF-FFH	+ 5 μM MBP
6.6	0.010 \pm 0.0009	0.010 \pm 0.002	0.011 \pm 0.001	0.012 \pm 0.0007
6.8	0.012 \pm 0.0009	0.012 \pm 0.0009	0.015 \pm 0.001	0.015 \pm 0.001
7.0	0.015 \pm 0.0012	0.016 \pm 0.0006	0.016 \pm 0.0006	0.017 \pm 0.001
7.2	0.017 \pm 0.0036	0.017 \pm 0.0002	0.018 \pm 0.001	0.020 \pm 0.002
7.4	0.021 \pm 0.0011	0.021 \pm 0.001	0.023 \pm 0.002	0.024 \pm 0.001

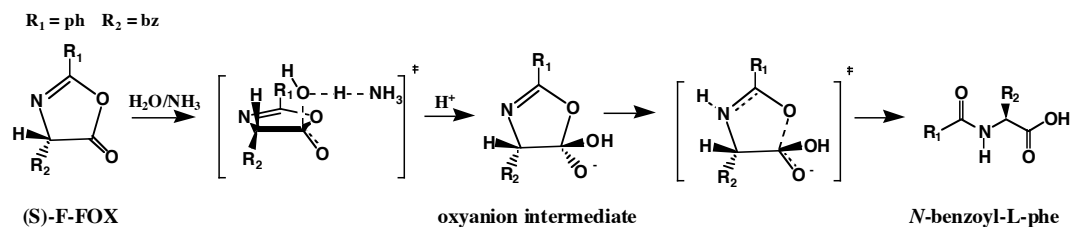


Figure A-1. Model system for dynamic kinetic resolution. Enantioselective hydrolysis of S-2-benzyl-4-phenyl-oxazolone-5-one ((S)-F-FOX).⁸

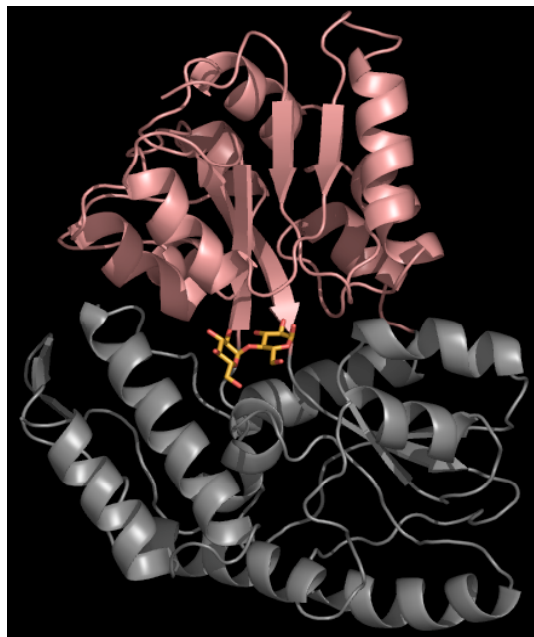


Figure A-2. Maltose binding protein structure. The scaffold for the design, maltose binding protein, in complex with maltose (pdb code: 1ANF).¹⁷

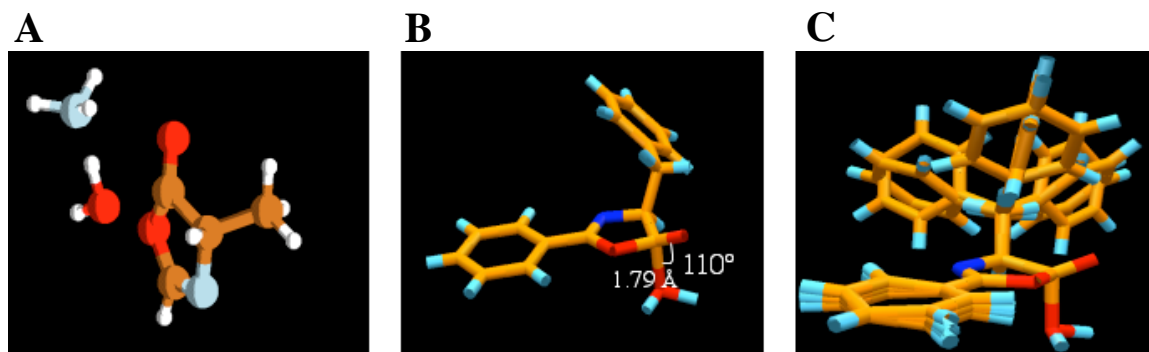


Figure A-3. (S)-F-FOX transition state structure. (A) The system for the *ab initio* calculation of the reaction transition state included a simplified (S)-F-FOX and a water molecule. NH_3 was added to activate the water. (B) Final transition state structure. (C) Rotamers of the transition state. The phenyl side chain can rotate 15° out of the plane of the oxazolone. The benzyl sidechain rotamers are based on the canonical backbone independent rotamers for phenylalanine.

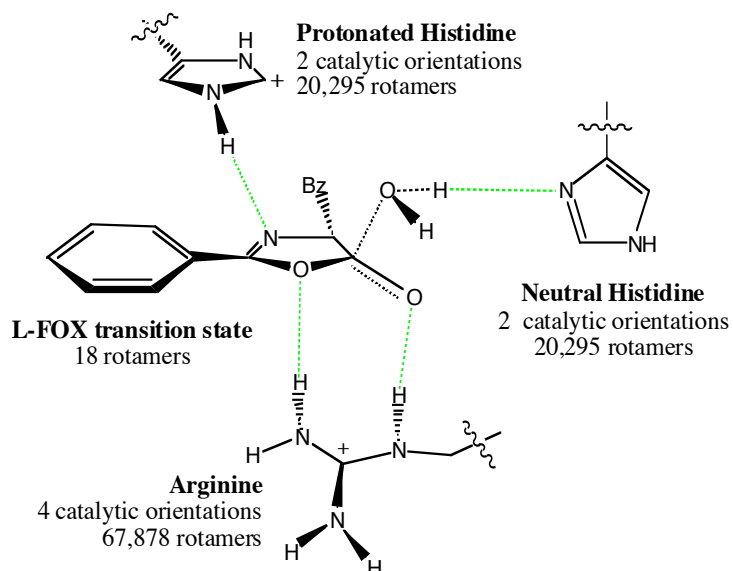


Figure A-4. Ideal active site contacts. Ideal hydrogen bond contacts between the desired catalytic residues and (S)-F-FOX hydrolysis transition state.

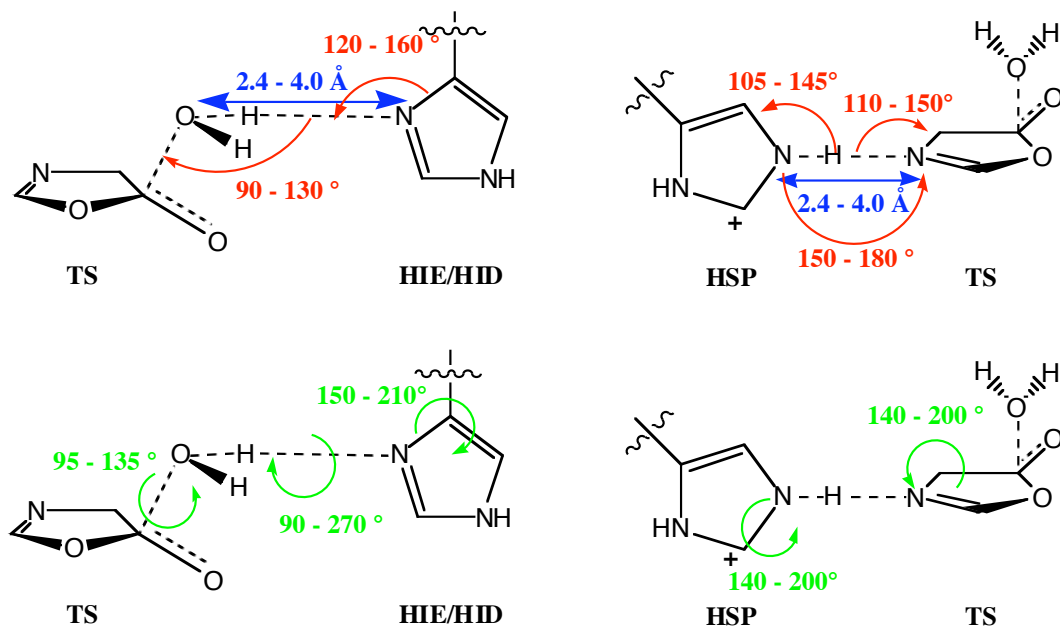


Figure A-5. Geometric constraints for the contacts between the catalytic residues and the (S)-F-FOX transition state (TS). Distance constraints are shown in blue, angle constraints are shown in red, and torsion constraints are shown in green. The transition state side chains were removed for clarity.

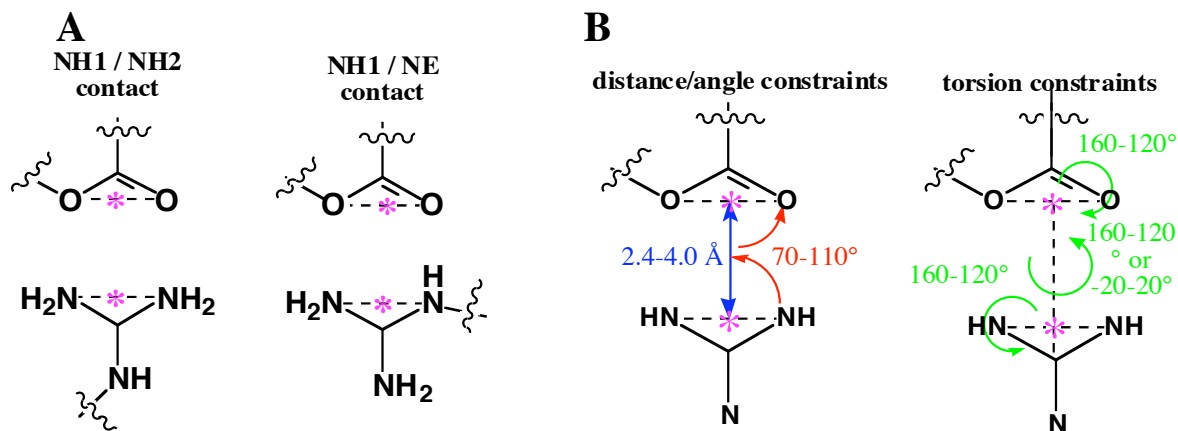


Figure A-6. Arginine-(S)-F-FOX geometric constraints. (A) Arginine can make four different double hydrogen bonding contacts to the transition state: NH1/oxazolone O and NH2/O; NH1/O and NH2/oxazolone O; NH1/oxazolone O and NE/O; NH1/O and NE/oxazolone O. Pseudo-atoms represented by pink stars. (B) Geometric constraints for the contacts between arginine and the transition state oxygens. Distance constraints are shown in blue, angle constraints are shown in red, and torsional constraints are shown in green. Pseudo-atoms are represented by pink stars.

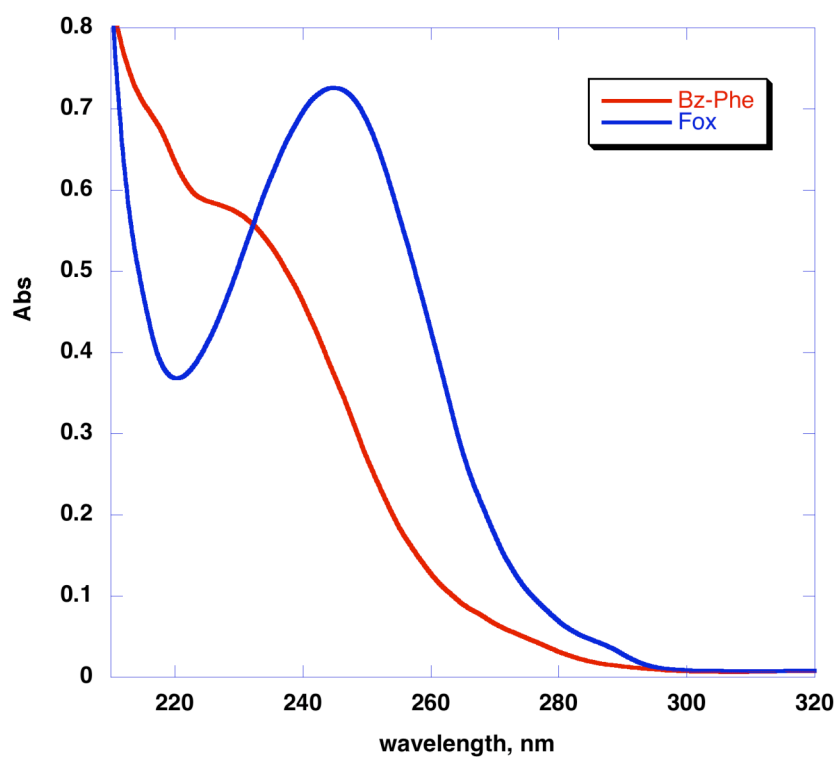


Figure A-7. UV-vis spectra of F-FOX and N-benzoyl-phenylalanine. λ_{\max} for F-FOX is 244.5 nm.

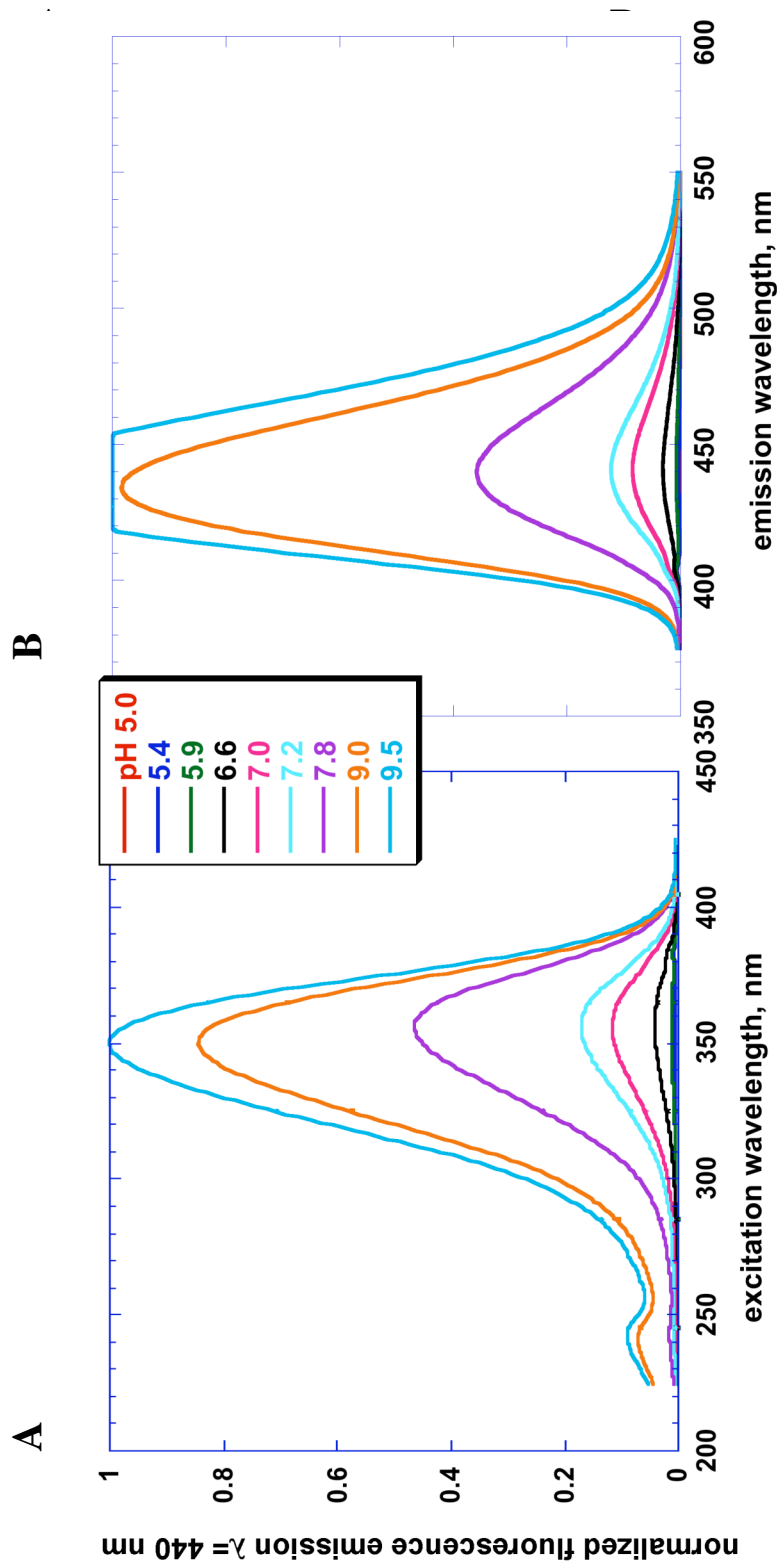


Figure A-8. Fluorescence of F-FOX. Wavelength scans were carried out using 4 μ M F-FOX in 10 mM potassium phosphate buffer (A) pH dependence of F-FOX fluorescence $\lambda_{em} = 440$ nm. (B) pH dependence of F-FOX fluorescence emission at $\lambda_{ex} = 356$ nm.

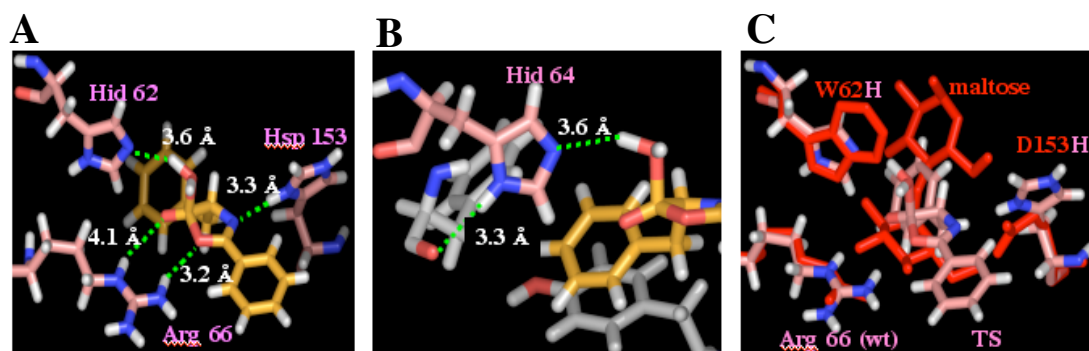


Figure A-9. Active site structure. (A) Chosen active site location and configuration. Hydrogen bonds are represented by dotted green lines. (B) Additional stabilization of Hid 64. (C) Designed active site residues (pink) overlaid with wild-type residues at those positions (red).

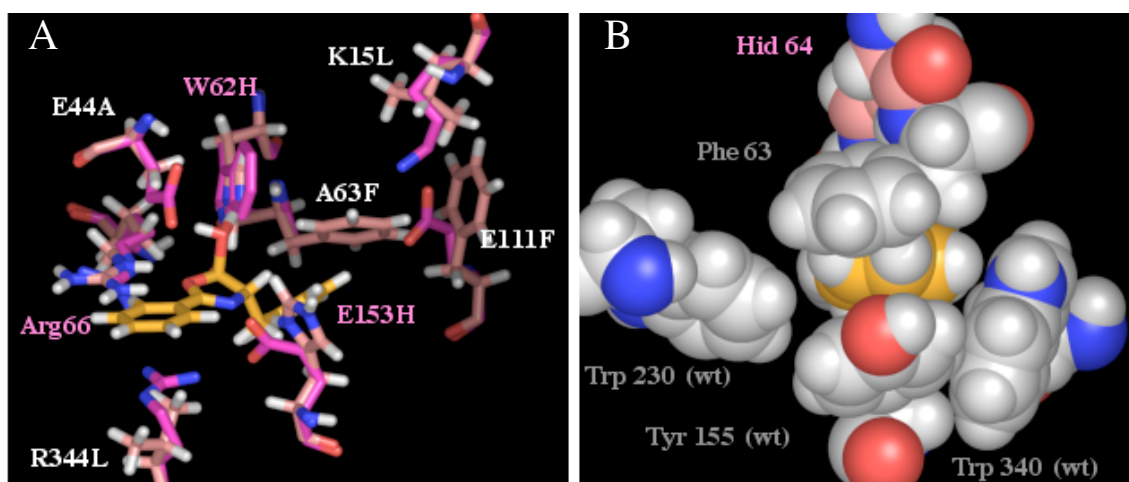


Figure A-10. Repacked active site. (A) The designed active site is shown in light pink and is overlaid with the wild-type binding pocket (magenta). The transition state structure is shown in yellow. (B) Space-filling representation of the active site. The benzyl side chain of the transition state is shown in yellow.

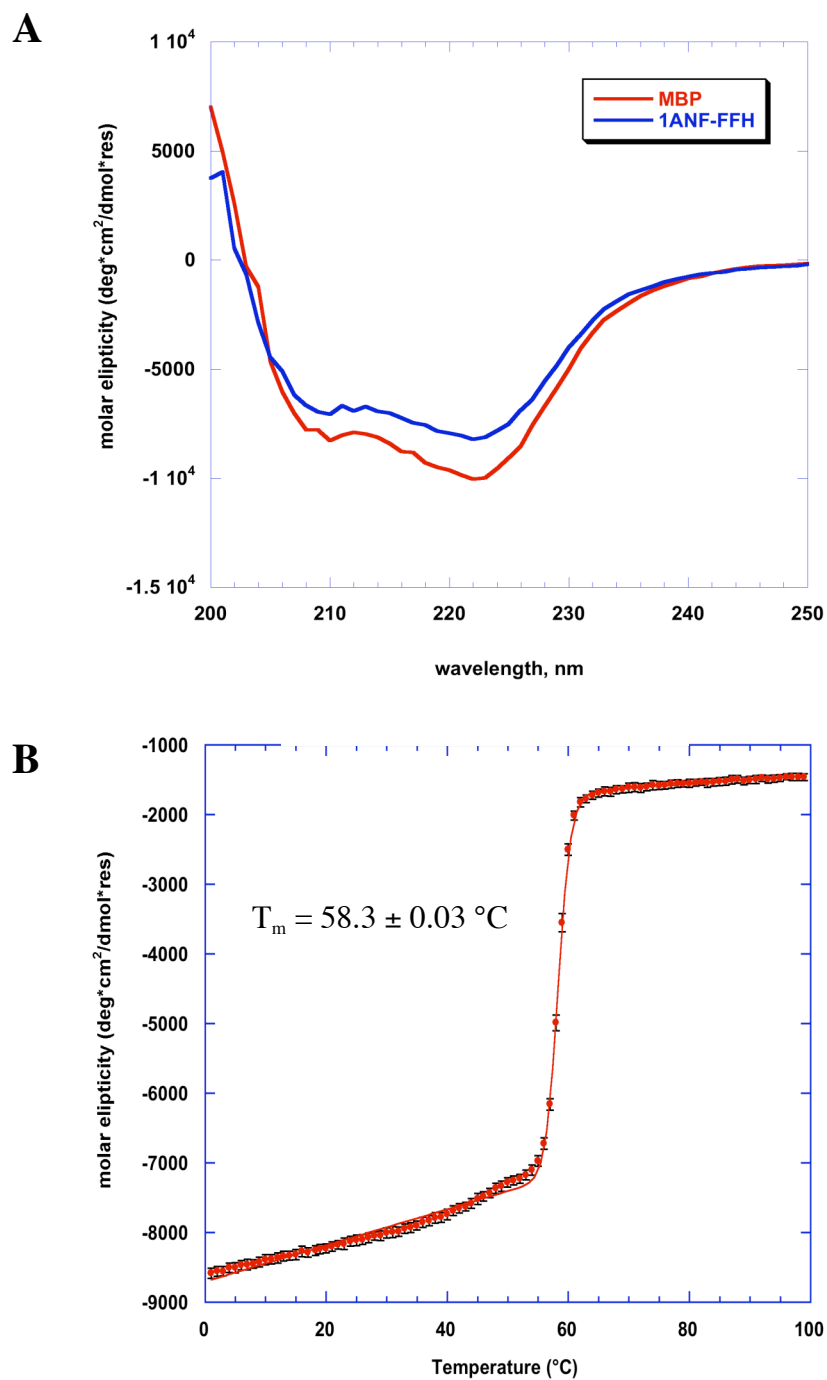


Figure A-11. 1ANF-FFH CD analysis. (A) CD wavelength scans of 1ANF-FFH compared to a scan for wild type MBP under identical conditions. (B) Thermal denaturation curve of 1ANF-FFH measured at 222 nm. All samples include 16.1 μM 1ANF-FFH, 20 mM KPi 50 mM NaCl, pH 7.4.

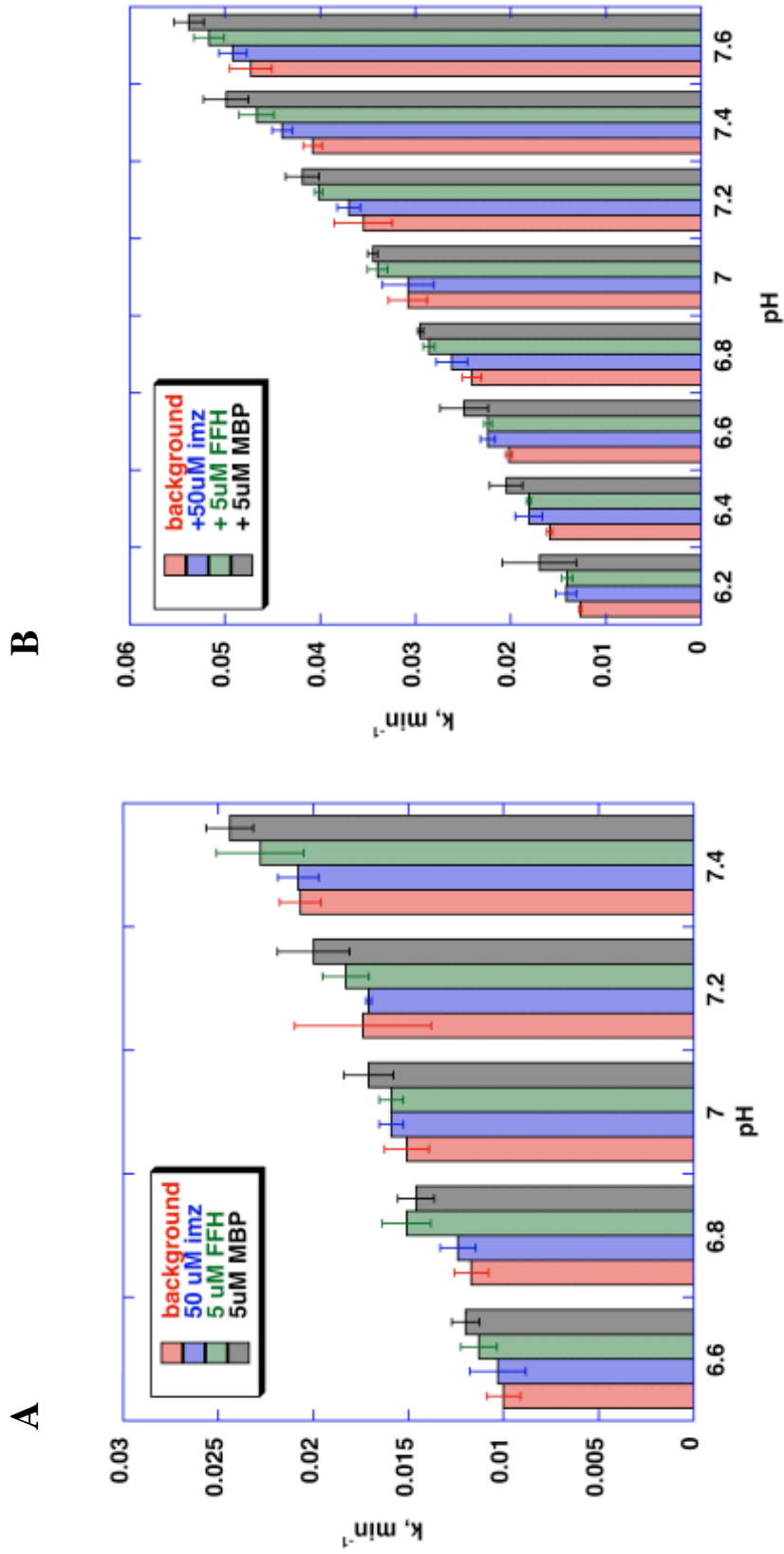
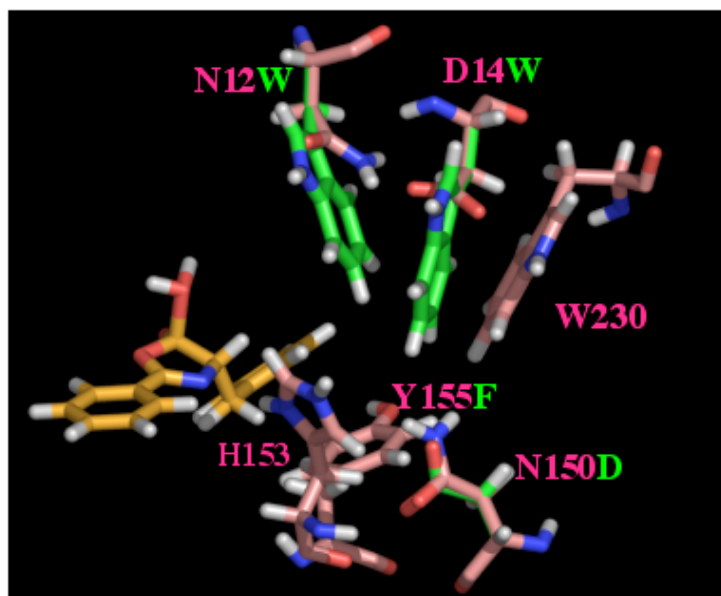


Figure A-12. F-FOX hydrolysis rate constants determined by UV-vis kinetics assays. The background rate constant was determined in the indicated buffer: (A) 10 mM KPi, 50mM NaCl or (B) 50 mM KPi, 50 mM NaCl. The rate constants for the hydrolysis of F-FOX in the indicated buffer in the presence of 50 μ M imidazole, 5 μ M IANF-FFH, and 5 μ M MBP are shown in blue, green, and black, respectively.



Mutation	Purpose
N12W + D14W	overall stabilization of binding pocket
N150D	stabilization of protonated form of H153
Y155F	overall stabilization of active site
I239W + A96W	shift of MBP equilibrium to closed conformation

Figure A-13. Additional potential beneficial mutations to 1ANF-FFH. The transition state is shown in yellow. Wild-type residues are shown in pink and mutations are shown in green.

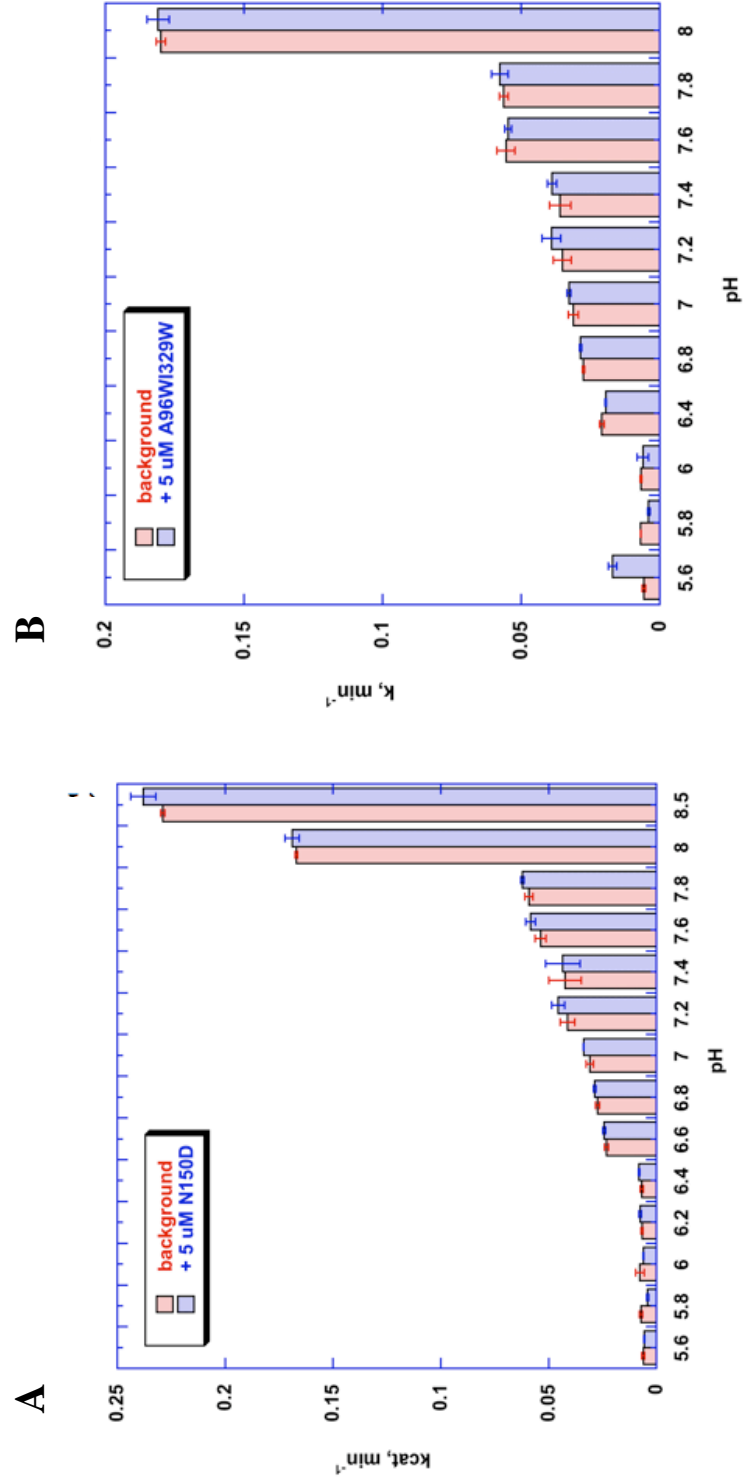


Figure A-14. 1ANF-FFH mutant apparent rate constants. The rate constants for (A) 1ANF-FFH N150D mutant and (B) 1ANF-FFH A96W/I329W double mutant were determined in 50 mM buffer, 50 mM NaCl at 25°C. No rate acceleration over background was seen for either variant under any condition tested.

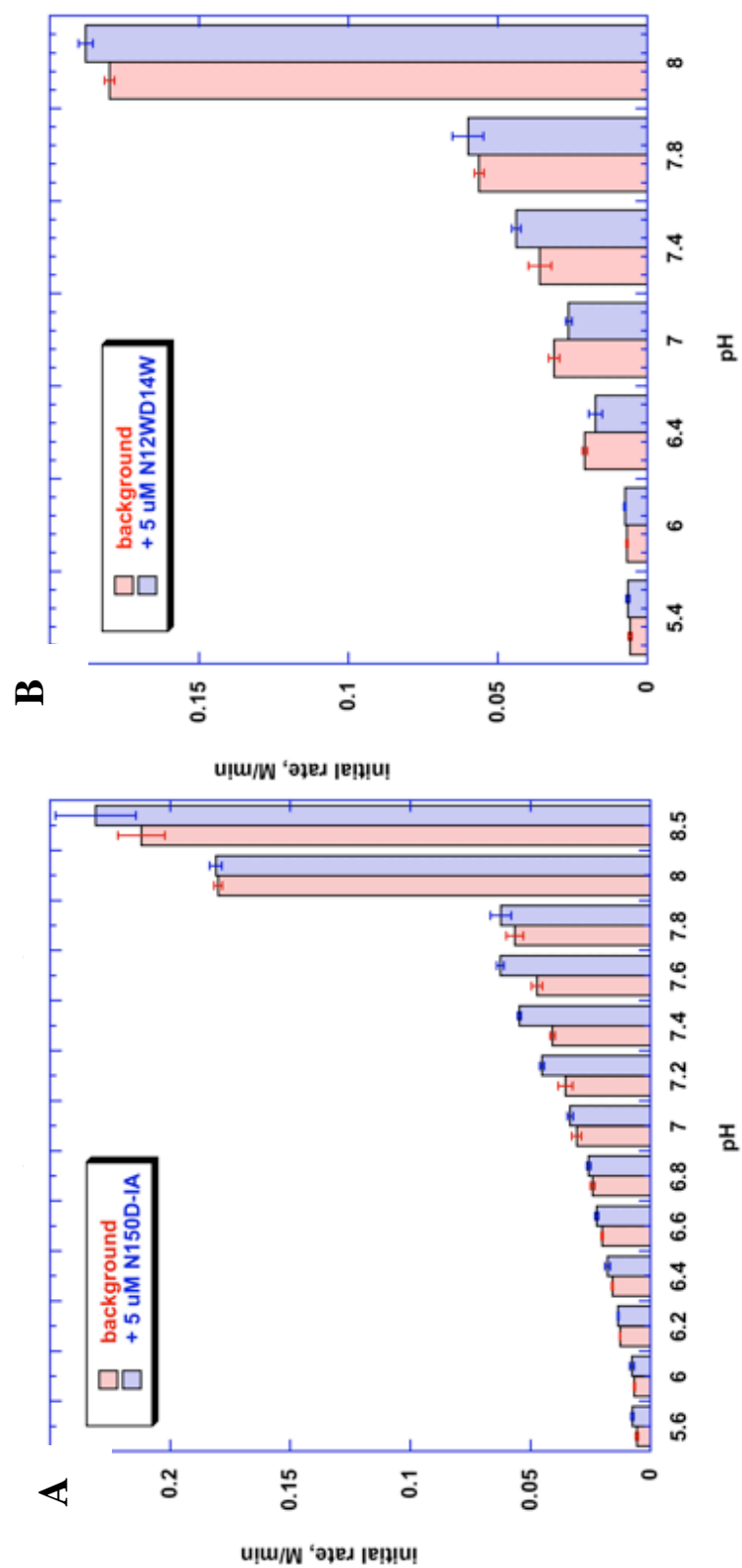


Figure A-15. 1ANF-FFH mutant apparent rate constants. The rate constants for: (A) 1ANF-FFH N150D/A96W/I329W triple mutant and (B) 1ANF-FFH N12W/D14W double mutant were determined in 50 mM buffer, 50 mM NaCl at 25°C. No rate acceleration over background was seen for either variant under any condition tested.